REPORT

Somatic *MAP3K3* mutation defines a subclass of cerebral cavernous malformation

Jiancong Weng,[1,2,11] Yingxi Yang,[3,11] Dong Song,[4,11] Ran Huo,[1,2,11] Hao Li,[1,2] Yiyun Chen,[4] Yoonhee Nam,[4] Qiuxia Zhou,[4] Yuming Jiao,[1,2] Weilun Fu,[1,2] Zihan Yan,[1,2] Jie Wang,[1,2] Hongyuan Xu,[1,2] Lin Di,[6] Jie Li,[7,8] Shuo Wang,[1,2] Jizong Zhao,[1,2] Jiguang Wang,[3,4,5,*] and Yong Cao[1,2,9,10,*]

Summary

Cerebral cavernous malformations (CCMs) are vascular disorders that affect up to 0.5% of the total population. About 20% of CCMs are inherited because of familial mutations in CCM genes, including *CCM1/KRIT1*, *CCM2/MGC4607*, and *CCM3/PDCD10*, whereas the etiology of a majority of simplex CCM-affected individuals remains unclear. Here, we report somatic mutations of *MAP3K3*, *PIK3CA*, *MAP2K7*, and CCM genes in CCM lesions. In particular, somatic hotspot mutations of *PIK3CA* are found in 11 of 38 individuals with CCMs, and a *MAP3K3* somatic mutation (c.1323C>G [p.Ile441Met]) is detected in 37.0% (34 of 92) of the simplex CCM-affected individuals. Strikingly, the *MAP3K3* c.1323C>G mutation presents in 95.7% (22 of 23) of the popcorn-like lesions but only 2.5% (1 of 40) of the subacute-bleeding or multifocal lesions that are predominantly attributed to mutations in the CCM1/2/3 signaling complex. Leveraging mini-bulk sequencing, we demonstrate the enrichment of *MAP3K3* c.1323C>G mutation in CCM endothelium. Mechanistically, beyond the activation of CCM1/2/3-inhibited ERK5 signaling, MEKK3 p.Ile441Met (*MAP3K3* encodes MEKK3) also activates ERK1/2, JNK, and p38 pathways because of mutation-induced MEKK3 kinase activity enhancement. Collectively, we identified several somatic activating mutations in CCM endothelium, and the *MAP3K3* c.1323C>G mutation defines a primary CCM subtype with distinct characteristics in signaling activation and magnetic resonance imaging appearance.

Cerebral cavernous malformations (CCMs [MIM: 116860]), the vascular dysplasia characterized by clusters of dilated capillaries and veins, affect 0.16%~0.5% of the overall population.[1,2] These lesions frequently lead to epileptic seizures, hemorrhagic strokes, headaches, or focal neurological deficits.[3,4] About 20% of CCMs are inherited in an autosomal dominant manner (familial CCMs), while 80% of CCMs occur without a positive family history (simplex CCMs).[5–7]

It is believed that approximately 78%–94% of familial CCMs are associated with loss-of-function mutations in one of the three CCM genes (i.e., *CCM1/KRIT1* [MIM: 604214], *CCM2/MGC4607* [MIM: 607929], and *CCM3/PDCD10* [MIM: 609118]).[8,9] In contrast, simplex CCMs could be caused by non-inherited factors (sporadic CCMs), *de novo* germline mutations, and incorrect diagnosis or incomplete penetrance of an autosomal dominant disorder in other family members.[10]

To uncover the genetic landscape of CCM, we applied deep whole-exome sequencing (WES) on fresh-frozen operative specimens with paired peripheral whole-blood samples from 38 affected individuals in the discovery cohort (Table S1). The procedures followed were in accordance with the ethical standards of the responsible committee on human experimentation (Beijing Tiantan Hospital, China), and the proper informed consent has been obtained (Figure S1A). Using MUTracer, a pipeline developed to prioritize somatic and germline mutations that are functional in a genetic disorder, we discovered four germline mutations affecting *CCM1* and *CCM3* and 16 nonsynonymous somatic mutations in *CCM1*, *CCM2*, *MAP3K3* (MIM: 602539), *PIK3CA* (MIM: 171834), and *MAP2K7* (MIM: 6030142) (Figures 1A and S1B, details provided in supplemental methods).

Consistent with previous studies,[8,9,11] we found that four out of six multi-lesion affected individuals harbored germline mutations of *CCM1* (c.1336C>T [p.Gln446*], c.756C>G [p.Tyr252*], and c.1664C>T [p.Ala555Val] [GenBank: NM_004912.4]) or *CCM3* (c.322C>T [p.Arg108*] [GenBank: NM_007217.4]) in the discovery cohort (Figure 1A). Somatic mutations were recently reported in a subgroup of simplex affected individuals.[12] Here, we confirmed that 19.4% (7/36) of individuals with simplex CCMs harbored somatic mutations in *CCM1* or *CCM2*. Notably, CCM-affected individual D13 harbored loss-of-function *CCM1* mutations at both the germline

Figure 1. Mutational landscape reveals a recurrent somatic *MAP3K3* mutation in CCM

(A) Somatic and germline mutations were identified from 38 CCMs in the discovery cohort. Both germline (with "G" in the center) and somatic alterations were included. "D" indicates the mutation was detected by ddPCR (droplet digital polymerase chain reaction). The lollipop plots at the bottom showed locations of identified mutations within *MAP3K3*, *CCM1*, and *PIK3CA* genes. The p value between CCM genes (*CCM1*, *CCM2*, and *CCM3*) and the *MAP3K3* c.1323C>G mutations was computed by Fisher's exact test.

(B) Mutation allele frequencies (MAFs) of *MAP3K3* c.1323C>G mutation detected by WES (whole-exome sequencing) and/or ddPCR with fresh-frozen samples (n = 9). The ddPCR experiments of each sample were repeated three times (technical replicates). Mean values of the three replicates were shown in the bar plot.

(C) Waterfall plot showed ranked MAFs of *MAP3K3* c.1323C>G mutation within the validation group (n = 25, MAF > 0). Mutational incidence of *MAP3K3* c.1323C>G detected by ddPCR was displayed by a pie chart.

(c.1336C>T [p.Gln446*]) and somatic (c.1651_1667del [p.Leu551SerfsTer11]) level, and affected individual D27 developed two somatic *CCM1* mutations (c.1417C>T [p.Gln473*] and c.703G>T [p.Gly235*]), providing clinical evidence for two-hit model of lesion genesis.[12,13]

In addition, we detected somatic *PIK3CA* mutations (c.1258T>C [p.Cys420Arg], c.1624G>A [p.Glu542Lys], c.1633G>A [p.Glu545Lys], c.3140A>G [p.His1047Arg], and c.3140A>T [p.His1047Leu] [GenBank: NM_006218. 4]) in 11 out of 38 individuals (Figure 1A). Moreover, a recurrent *MAP3K3* mutation (c.1323C>G [p.Ile441Met] [GenBank: NM_002401.5]) was detected in eight of 36 simplex CCM-affected individuals (22.2%) on the basis of

WES, and the mutational allele frequency (MAF) ranged from 0.6% to 15% (Figures 1B and S1C). Interestingly, this mutation was previously found in verrucous venous malformation, a rare vascular anomaly underlying hyperkeratotic skin.[14] In our cohort, this mutation was mutually exclusive with mutations affecting CCM genes, implying an alternative role of *MAP3K3* c.1323C>G in CCM pathogenesis.

To verify the presence of somatic *MAP3K3* c.1323C>G, we utilized droplet digital polymerase chain reaction (ddPCR) on fresh-frozen samples and blood controls of the discovery cohort (Figures S1D and S2). All eight *MAP3K3* c.1323C>G mutant affected individuals detected
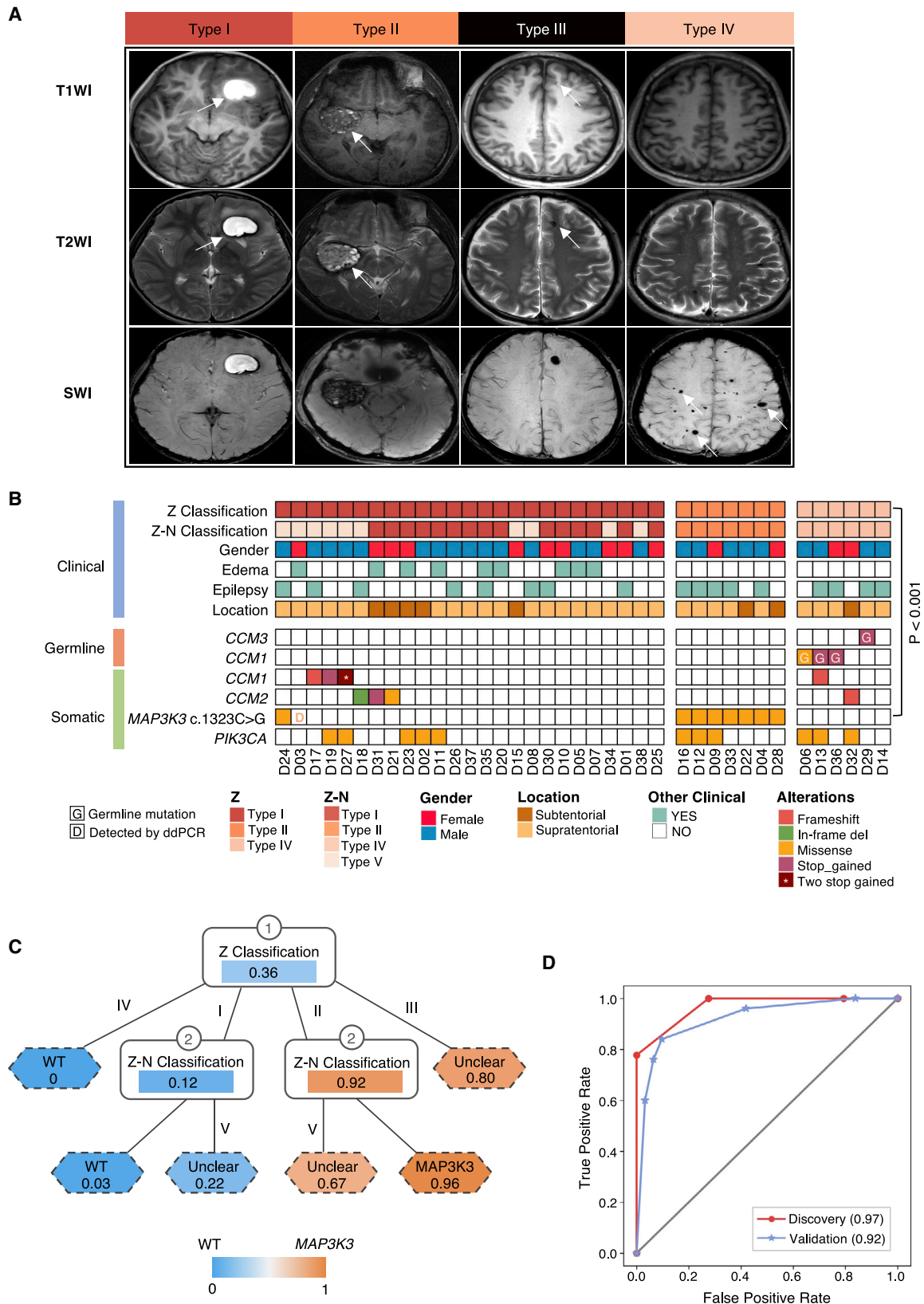
Figure 2. Somatic *MAP3K3* c.1323C>G mutation is related to the popcorn-like imaging appearance of CCM

(A) Representative imaging manifestation of CCM types (I–IV) based on Zabramski classification (Z classification). Type I, type II, and type III are respectively presented as hyperintense, typical mulberry, and a small punctuate lesions on T1-weighted imaging and T2-weighted imaging; type IV demonstrates multiple punctuate lesions on susceptibility-weighted imaging sequence.

by WES were confirmed by ddPCR, and the MAFs of the two schemes were highly correlated (r = 0.94, Figures 1B and S1E). With higher sensitivity, ddPCR detected *MAP3K3* c.1323C>G in one more affected individual (D03) with MAF = 0.09% (0.06%–0.12%, Figure S2). No more *MAP3K3* c.1323C>G mutations were detected in the remaining samples. The matched blood samples were negative for *MAP3K3* c.1323C>G mutation with 0 positive droplet. To check whether *MAP3K3* c.1323C>G is detectable in archived formalin-fixed paraffin-embedded (FFPE) samples, we applied ddPCR to FFPE samples of the discovery cohort (n = 36) and demonstrated that this approach could achieve 100% accuracy in detecting *MAP3K3* c.1323C>G (Figure S1F). Accordingly, we examined *MAP3K3* c.1323C>G mutation in an independent cohort consisting of FFPE sample of 75 simplex CCM-affected individuals. To control false negatives, 56 samples with >5,000 total droplets were enrolled in the validation cohort (Table S2). To decrease false positives, only mutations supported by >6 positive droplets were reported. As a result, we detected *MAP3K3* c.1323C>G mutation in 25/56 CCM-affected individuals (44.6%), and the MAF ranged from 0.034% to 13.47% (Figures 1C and S3). Taken together, we found that 34 of 92 individuals with simplex CCMs (37.0%) harbor somatic *MAP3K3* c.1323C>G mutation. Following the same protocol, we also analyzed FFPE samples of normal superficial temporal artery obtained from four control individuals who were undergoing standard craniotomy procedure. The fractional abundance of *MAP3K3* c.1323C>G in these control FFPE tissue samples did not exceed 0.026% (three out of 7,680 droplets).

We next investigated the clinical implication of *MAP3K3* c.1323C>G. Zabramski classified CCM lesions into four subtypes on the basis of magnetic resonance imaging (MRI):[15] type I shows subacute bleeding, type II exhibits popcorn-like lesions, type III is featured by chronic hemorrhage, and type IV corresponds to dot-sized multifocal lesions (Figure 2A). Using Zabramski's method, we classified enrolled individuals into four subtypes (details provided in supplemental methods, Figures S4 and S5). In concordance with previous studies,[9,16] Zabramski type IV was associated with the germline mutations of CCM genes (p = 0.0002 by Fisher's exact test, Figures 2B and S6A). Remarkably, combining discovery and validation cohorts, the detected *MAP3K3* c.1323C>G mutation occurred only in 6/52 type I and none of 11 type IV CCM-affected individuals but was present in 24/26 type II and 4/5 type III affected individuals (Figures 2B and S6B–S6F).

We then interrogated whether the imaging-based diagnosis could be used to infer genetic mutations. To achieve a more comprehensive MRI evaluation, we applied Zabramski-Nikoubashman classification,[17] a calibrated approach that recategorizes a subset of original type I/II lesions with gross extralesional hemorrhage into type V. Interestingly, based on the calibrated scheme, five type I *MAP3K3* c.1323C>G mutant affected individuals (D24, D03, V26, V28, and V60) and one type II *MAP3K3* wild-type (WT) CCM-affected individual (V53) were grouped as type V (Figure S7A). Remarkably, *MAP3K3* c.1323C>G mutation was now in 22 of 23 popcorn-like lesions (p = 6.7×10^{-12}), while rarely in type I (one of 29, p = 4.2×10^{-6}) or type IV (none of 11, p = 6.4×10^{-3}) lesions (Figures S7B–S7D), providing compelling evidence to support a rule of imaging-genetics association between *MAP3K3* c.1323C>G mutation and popcorn-like imaging characteristics. Moreover, we described a two-step decision tree model to infer *MAP3K3* genotype on the basis of the radiological evaluation (Figure 2C). This model achieved an area under the receiver operating characteristic curve (AUC ROC) of 0.97 in the discovery cohort and 0.92 in the validation cohort, providing an accurate noninvasive guideline for evaluating molecular etiology via MRI (Figure 2D). The prediction of mutations in *PIK3CA* and CCM genes were less accurate (Figures S8A–S8D).

To explore p.Ile441Met function, we first gathered the MEKK3 (*MAP3K3* encodes MEKK3) sequences from *Homo sapiens* (UniProt: Q99759-1, Figure S9) and 31 other vertebrates to study evolutionary conservation of this protein. We found that the kinase domain of MEKK3 is highly conserved, and the p.Ile441Met variant occurred in a 100% conserved position at the center of the β5 strand of the N-lobe of the kinase domain (Figures 3A and S10). We next built WT and p.Ile441Met variant 3D structural models of the MEKK3 kinase domain in complex with a cofactor ATP-2Mg^{2+} through homology modeling (details provided in supplemental methods). In the modeled structure (Figure 3B), the variant residue Met441 interacts with the hydrophobic regulatory spine essential for activities of all protein kinases on one side and with Met443, which is known as a gatekeeper linking the catalytic spine and regulatory spine of the active form of kinases on the other side.[18,19] To explore impact of p.Ile441Met variant on kinase activity, a phosphorylation-site-containing substrate peptide (312-IAKTYVG-318)[20] extracted from the MEKK3-downstream protein MEK5 was docked into the predicted MEKK3 models. Subsequently, we performed 500-ns all-atom molecular dynamics (MD) simulations and generated ten independent trajectories for WT and variant MEKK3 catalytic reaction complexes, respectively (Figures S11A and S11B). While little structural difference was observed in the overall conformation (atomic Cα

(B) Clinical and mutational profiles of CCMs in discovery cohort (n = 38). Z and Z-N indicate Zabramski and Zabramski-Nikoubashman, respectively. p value was calculated by Fisher's exact test.
(C) The two-step decision tree model to predict *MAP3K3* c.1323C>G mutation on the basis of radiological evaluation. Probability of *MAP3K3* c.1323C>G mutation was labeled in each node.
(D) Receiver operating characteristic curve showing model performance in the discovery cohort (n = 38) and the validation cohort (n = 56).
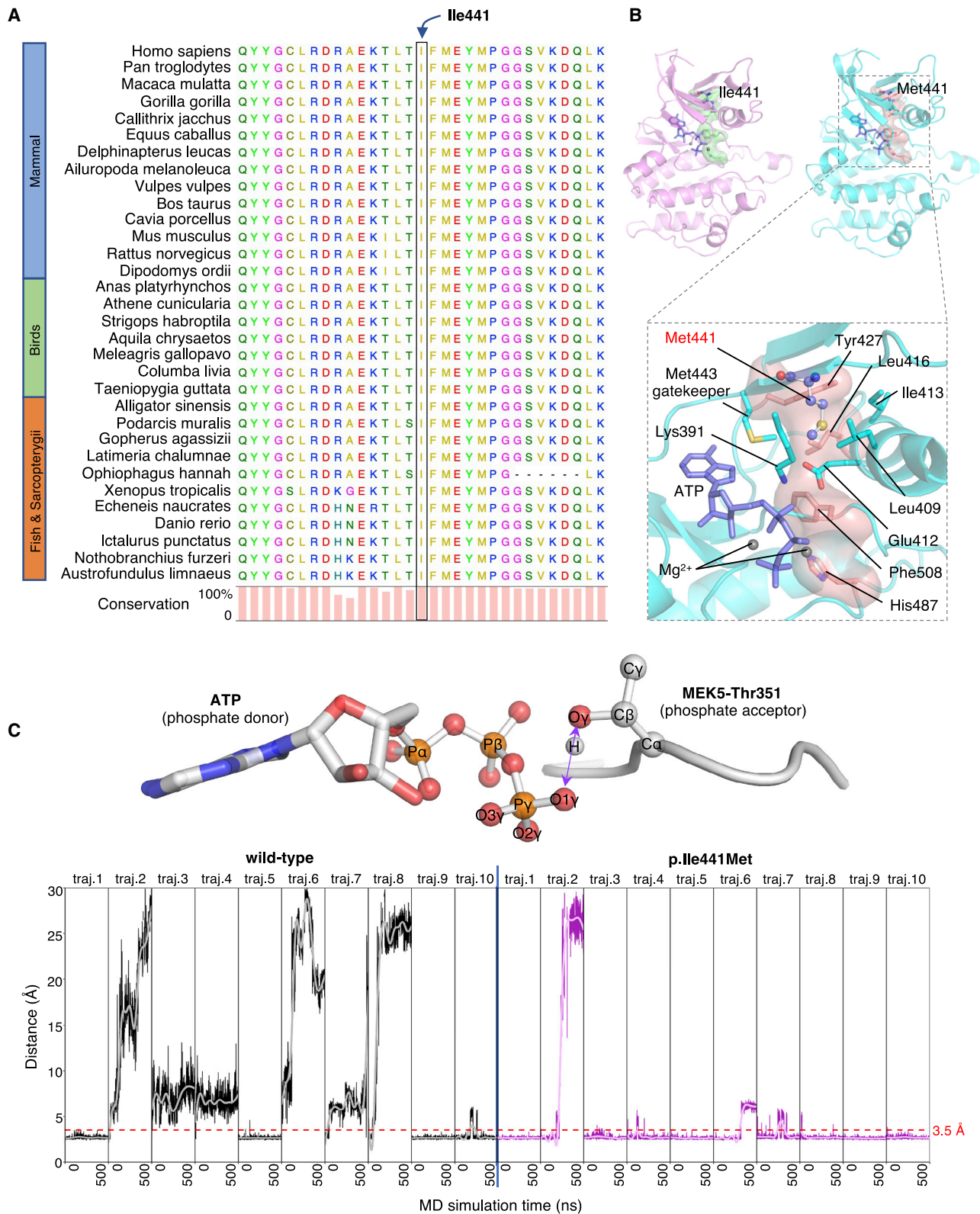
Figure 3. p.Ile441Met variant occurred on a conserved site of the MEKK3 kinase domain that might enhance its substrate binding

(A) Multiple sequence alignment of MEKK3 showed that the observed variant position Ile441 is 100% conserved among 32 different species.

(B) Homology-modeled structure of MEKK3^{WT} (violet) and MEKK3 p.Ile441Met (cyan). The highlighted local conformation of MEKK3 p.Ile441Met showed that the variant residue Met441 interacts with the hydrophobic regulatory spine (rendered in salmon) on one side and with the gatekeeper Met443 on the other side.

(legend continued on next page)

RMSD 1.631 Å) (Figure S11C), local conformational comparisons showed that the variant Met441 had a shorter distance to Leu409 but a longer distance to Leu416 (Figure S12). Moreover, the substrate peptide in the MEKK3[WT] system was prone to escape from the substrate binding site compared to that in MEKK3 p.Ile441Met (Figure 3C). These results collectively implied that the p.Ile441Met variant may enhance MEKK3 kinase activity by promoting its substrate binding.

To identify the specific cell types harboring the detected somatic mutations, we enriched CD45−/CD31+ cells (endothelial cells) and CD45−/CD31−/CD146+ cells (mural cells) in fresh CCM lesions from three individuals, followed by mini-bulk sequencing (details provided in supplemental methods). MAFs based on mini-bulk WES of endothelial cells and mural cells were compared to that of bulk WES. We found that somatic mutations showed superior specificity within endothelial cells compared with mural cells (Figure 4A). We next compared the mini-bulk RNA sequencing data of MAP3K3 c.1323C>G mutant affected individuals (D12 and D09) with that of MAP3K3-WT-affected individual D11 (Figure S13A). We found upregulation of PDGFRB (MIM: 173410), FGF1 (MIM: 131220), FGFR2 (MIM: 176943), GPER1 (MIM: 601805), MT3 (MIM: 139255), NDRG4 (MIM: 614463), and TREM2 (MIM: 605086) expression in MAP3K3 c.1323C>G mutant endothelial cells, indicating an activation of ERK1 and ERK2 cascades.

Finally, we investigated the change of downstream pathways in vitro. We infected human umbilical vein endothelial cells (HUVECs) and human embryonic kidney 293 (HEK293) with lentivirus encoding the MEKK3[WT] or MEKK3 p.Ile441Met. MEKK3 p.Ile441Met variant cells exhibited exacerbated activation of the downstream MEK5-ERK5 signaling, which has been considered to play an important role in the pathogenesis of CCMs (Figures 4B and S13B).[22–24] In addition, we found increased phosphorylation in MEKK3 p.Ile441Met variant HUVECs in ERK1/2, MEK6-p38, and JNK (Figures 4C and S13C). These results suggested that MEKK3 p.Ile441Met activates additional MEKK3 downstream signaling pathways. We further examined whether the MEKK3 p.Ile441Met activated signaling pathways can be influenced by loss-of-function mutation in CCM2, which has been reported to alleviate the inhibition of MEKK3 and activates the MEKK3-MEK5-ERK5 signaling pathway that drives CCM formation.[22,25] Interestingly, we found that knockdown of CCM2 in HUVECs activated the MEK5-ERK5 signaling but not ERK1/2, JNK, or MEK6-p38 (Figures 4D and S13D). Taken together, our results implied that compared with the loss-of-function of CCM genes, MEKK3 p.Ile441-Met promotes CCM through distinct molecular mechanisms that may contribute to the phenotypic differences between subtypes.

In summary, we report MAP3K3 c.1323C>G, a somatic mutation detected in over 95% of the popcorn-like CCM subtype, and showed that one single activating genetic alteration is capable of triggering severe phenotypic abnormalities that are detectable under radiological evaluation. Considering the difficulties of intracranial operations, the rule of image-genetics association we described in CCM provides a practical guideline that evaluates the molecular etiology of CCM individuals in a non-invasive way. Although we have identified functional genetic alterations in a majority of Zabramski type II–IV CCM lesions, only about half of type I affected individuals contained mutations, leaving the genetic causes of the other half an open challenge to be addressed.

Notably, somatic activating PIK3CA mutations were detected simultaneously with the somatic mutations in MAP3K3 or CCM genes in at least seven CCM-affected individuals (Figure 1A). To explore the association between PIK3CA mutations and other mutations, we compared the MAF of different genes in the same samples. Using WES, we found that MAFs of somatic PIK3CA mutations were higher than mutations affecting MAP3K3 or CCM1/2 in six out of seven individuals (Figure S14A). Statistically, PIK3CA mutations have slightly higher MAFs (p value = 0.086 by paired t test), implying PIK3CA mutation might occur as an early event in case that these multiple somatic mutations were needed by the same endothelial cells. The same trend was also observed in mini-bulk sequencing data, especially in the comparison of MAF between MAP3K3 c.1323C>G and PIK3CA c.3140A>G in affected individual D12 (Figure S14B, p = 0.01 by proportion Z test). These observations implied the occurrence of endothelial cell clonal expansion and therefore suggested a potential multiple-hit mechanism within the endothelial cell population. More functional studies should be performed to explore the role of PIK3CA and to verify whether these two different pathways need to be activated in the same cell for CCM pathogenesis.

Although our study presented an association with a specific mutation and Zabramski classification lesions at one point of time, it would be of great value to explore the correlation between MAP3K3 c.1323C>G mutation and the clinical course before surgery, considering that the untreated clinical course of the CCM is a critical factor guiding treatment decisions. Previous studies reported dynamic transformations among Zabramski type I, type II, and type III via radiological follow-up.[26,27] Therefore, a

---

(C) The comparison of MEKK3[WT] and MEKK3 p.Ile441Met in the distance between Thr315 Oγ of MEK5 substrate peptide and three Oγ of ATP in independent MD simulation trajectories. To allow phosphate transfer reaction, the phosphate group donor ATP and the phosphate group acceptor MEK5-Thr315 must have native contacts, which were usually defined by minimum heavy-atom separation (Thr315 Oγ–ATP Oγ in this case) < 3.5 Å.[21] The MD simulations showed that the Thr315 Oγ–ATP Oγ distance in six out of ten trajectories in MEKK3[WT] exceeds 3.5 Å (red dash line) in most of the simulation time. In contrast, the distance in nine out of ten trajectories in MEKK3 p.Ile441Met was mostly less than 3.5 Å, indicating an increased substrate binding ability by the p.Ile441Met variant.
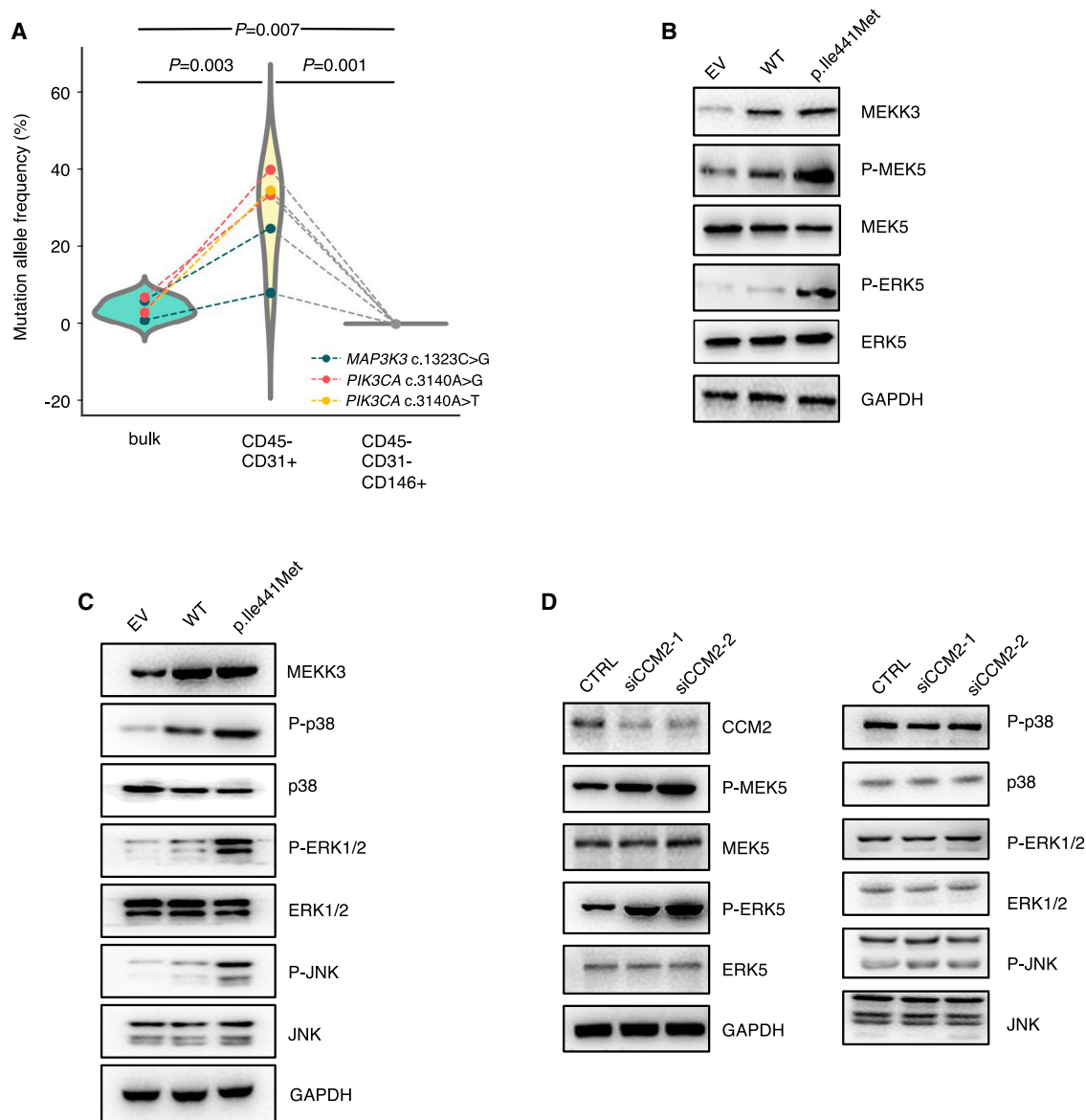
Figure 4. Somatic *MAP3K3* mutation activated MEKK3 signaling in endothelial cells
(A) Violin plots demonstrating mutational allele frequencies in bulk and mini-bulk DNA sequencing. In this analysis, three individuals (D11, D12, and D09) were utilized. p values were calculated by Wilcoxon rank-sum test.
(B and C) Immunoblots of human umbilical vein endothelial cells (HUVECs) infected by lentivirus encoding *MAP3K3*-WT, or *MAP3K3* c.1323C>G mutation, or empty vector (EV). (B) showed increased phosphorylation of ERK5 and MEK5 in MEKK3-Ile441Met variant HUVECs. (C) showed increased phosphorylation of p38, ERK1/2, and JNK in MEKK3 p.Ile441Met variant HUVECs.
(D) Immunoblots of CCM2 knockdown HUVECs showed increased phosphorylation of ERK5 and MEK5 but not p38, ERK1/2, or JNK.

prospective longitudinal study integrating genomics and imaging is crucially needed to consolidate our findings. On the other hand, possible longitudinal genetic studies in animal models will reveal mutational dynamics and deepen our understanding of how somatic mutations regulate CCM formation and development.

Data and code availability

The datasets supporting the current study have not been deposited in a public repository because of institutional ethics restrictions but are available from the corresponding author on request. The open-source code and corresponding instructions are available at https://github.com/sheenaseven/MUTracer.

Supplemental information

Supplemental information can be found online at https://doi.org/10.1016/j.ajhg.2021.04.005.

Web resources

GenBank, https://www.ncbi.nlm.nih.gov/genbank/
HUGO nomenclature committee, https://www.genenames.org/
Mutalyzer, https://mutalyzer.nl
Online Mendelian Inheritance in Man (OMIM), https://www.omim.org/
Sequence Variant Nomenclature, http://varnomen.hgvs.org/

References

1. Morris, Z., Whiteley, W.N., Longstreth, W.T., Jr., Weber, F., Lee, Y.C., Tsushima, Y., Alphs, H., Ladd, S.C., Warlow, C., Wardlaw, J.M., and Al-Shahi Salman, R. (2009). Incidental findings on brain magnetic resonance imaging: systematic review and meta-analysis. BMJ 339, b3016.

2. Al-Holou, W.N., O'Lynnger, T.M., Pandey, A.S., Gemmete, J.J., Thompson, B.G., Muraszko, K.M., Garton, H.J., and Maher, C.O. (2012). Natural history and imaging prevalence of cavernous malformations in children and young adults. J. Neurosurg. Pediatr. 9, 198–205.

3. Al-Shahi Salman, R., Berg, M.J., Morrison, L., Awad, I.A.; and Angioma Alliance Scientific Advisory Board (2008). Hemorrhage from cavernous malformations of the brain: definition and reporting standards. Stroke 39, 3222–3230.

4. Stapleton, C.J., and Barker, F.G., 2nd. (2018). Cranial Cavernous Malformations: Natural History and Treatment. Stroke 49, 1029–1035.

5. Riant, F., Bergametti, F., Ayrignac, X., Boulday, G., and Tournier-Lasserve, E. (2010). Recent insights into cerebral cavernous malformations: the molecular genetics of CCM. FEBS J. 277, 1070–1075.

6. Akers, A., Al-Shahi Salman, R., A Awad, I., Dahlem, K., Flemming, K., Hart, B., Kim, H., Jusue-Torres, I., Kondziolka, D., Lee, C., et al. (2017). Synopsis of Guidelines for the Clinical Management of Cerebral Cavernous Malformations: Consensus Recommendations Based on Systematic Literature Review by the Angioma Alliance Scientific Advisory Board Clinical Experts Panel. Neurosurgery 80, 665–680.

7. Chohan, M.O., Marchiò, S., Morrison, L.A., Sidman, R.L., Cavenee, W.K., Dejana, E., Yonas, H., Pasqualini, R., and Arap, W. (2019). Emerging Pharmacologic Targets in Cerebral Cavernous Malformation and Potential Strategies to Alter the Natural History of a Difficult Disease: A Review. JAMA Neurol. 76, 492–500.

8. Denier, C., Labauge, P., Bergametti, F., Marchelli, F., Riant, F., Arnoult, M., Maciazek, J., Vicaut, E., Brunereau, L., Tournier-Lasserve, E.; and Société Française de Neurochirurgie (2006). Genotype-phenotype correlations in cerebral cavernous malformations patients. Ann. Neurol. 60, 550–556.

9. Labauge, P., Denier, C., Bergametti, F., and Tournier-Lasserve, E. (2007). Genetics of cavernous angiomas. Lancet Neurol. 6, 237–244.

10. Spiegler, S., Rath, M., Paperlein, C., and Felbor, U. (2018). Cerebral Cavernous Malformations: An Update on Prevalence, Molecular Genetic Analyses, and Genetic Counselling. Mol. Syndromol. 9, 60–69.

11. Spiegler, S., Najm, J., Liu, J., Gkalympoudis, S., Schröder, W., Borck, G., Brockmann, K., Elbracht, M., Fauth, C., Ferbert, A., et al. (2014). High mutation detection rates in cerebral cavernous malformation upon stringent inclusion criteria: one-third of probands are minors. Mol. Genet. Genomic Med. 2, 176–185.

12. McDonald, D.A., Shi, C., Shenkar, R., Gallione, C.J., Akers, A.L., Li, S., De Castro, N., Berg, M.J., Corcoran, D.L., Awad, I.A., and Marchuk, D.A. (2014). Lesions from patients with sporadic cerebral cavernous malformations harbor somatic mutations in the CCM genes: evidence for a common biochemical pathway for CCM pathogenesis. Hum. Mol. Genet. 23, 4357–4370.

13. Akers, A.L., Johnson, E., Steinberg, G.K., Zabramski, J.M., and Marchuk, D.A. (2009). Biallelic somatic and germline mutations in cerebral cavernous malformations (CCMs): evidence for a two-hit mechanism of CCM pathogenesis. Hum. Mol. Genet. 18, 919–930.

14. Couto, J.A., Vivero, M.P., Kozakewich, H.P.W., Taghinia, A.H., Mulliken, J.B., Warman, M.L., and Greene, A.K. (2015). A somatic MAP3K3 mutation is associated with verrucous venous malformation. Am. J. Hum. Genet. 96, 480–486.

15. Zabramski, J.M., Wascher, T.M., Spetzler, R.F., Johnson, B., Golfinos, J., Drayer, B.P., Brown, B., Rigamonti, D., and Brown, G. (1994). The natural history of familial cavernous malformations: results of an ongoing study. J. Neurosurg. 80, 422–432.

16. Clatterbuck, R.E., Elmaci, I., and Rigamonti, D. (2001). The nature and fate of punctate (type IV) cavernous malformations. Neurosurgery 49, 26–30, discussion 30–32.

17. Nikoubashman, O., Di Rocco, F., Davagnanam, I., Mankad, K., Zerah, M., and Wiesmann, M. (2015). Prospective Hemorrhage Rates of Cerebral Cavernous Malformations in Children and Adolescents Based on MRI Appearance. AJNR Am. J. Neuroradiol. 36, 2177–2183.

18. Hu, J., Yu, H., Kornev, A.P., Zhao, J., Filbert, E.L., Taylor, S.S., and Shaw, A.S. (2011). Mutation that blocks ATP binding creates a pseudokinase stabilizing the scaffolding function of kinase suppressor of Ras, CRAF and BRAF. Proc. Natl. Acad. Sci. USA 108, 6067–6072.

19. Taylor, S.S., and Kornev, A.P. (2011). Protein kinases: evolution of dynamic regulatory proteins. Trends Biochem. Sci. 36, 65–77.

20. Zhou, G., Bao, Z.Q., and Dixon, J.E. (1995). Components of a new human protein kinase signal transduction pathway. J. Biol. Chem. 270, 12665–12669.

21. Best, R.B., Hummer, G., and Eaton, W.A. (2013). Native contacts determine protein folding mechanisms in atomistic simulations. Proc. Natl. Acad. Sci. USA *110*, 17874–17879.

22. Zhou, Z., Tang, A.T., Wong, W.-Y., Bamezai, S., Goddard, L.M., Shenkar, R., Zhou, S., Yang, J., Wright, A.C., Foley, M., et al. (2016). Cerebral cavernous malformations arise from endothelial gain of MEKK3-KLF2/4 signalling. Nature *532*, 122–126.

23. Cuttano, R., Rudini, N., Bravi, L., Corada, M., Giampietro, C., Papa, E., Morini, M.F., Maddaluno, L., Baeyens, N., Adams, R.H., et al. (2016). KLF4 is a key determinant in the development and progression of cerebral cavernous malformations. EMBO Mol. Med. *8*, 6–24.

24. Tang, A.T., Choi, J.P., Kotzin, J.J., Yang, Y., Hong, C.C., Hobson, N., Girard, R., Zeineddine, H.A., Lightle, R., Moore, T., et al. (2017). Endothelial TLR4 and the microbiome drive cerebral cavernous malformations. Nature *545*, 305–310.

25. Fisher, O.S., Deng, H., Liu, D., Zhang, Y., Wei, R., Deng, Y., Zhang, F., Louvi, A., Turk, B.E., Boggon, T.J., and Su, B. (2015). Structure and vascular function of MEKK3-cerebral cavernous malformations 2 complex. Nat. Commun. *6*, 7937–7947.

26. Clatterbuck, R.E., Moriarity, J.L., Elmaci, I., Lee, R.R., Breiter, S.N., and Rigamonti, D. (2000). Dynamic nature of cavernous malformations: a prospective magnetic resonance imaging study with volumetric analysis. J. Neurosurg. *93*, 981–986.

27. Flemming, K.D., Kumar, S., Lanzino, G., and Brinjikji, W. (2019). Baseline and Evolutionary Radiologic Features in Sporadic, Hemorrhagic Brain Cavernous Malformations. AJNR Am. J. Neuroradiol. *40*, 967–972.